

Rotating Relativistic Thin Disks

*Guillermo A. González**

Escuela de Física
Universidad Industrial de Santander
A.A. 678, Bucaramanga, Colombia

and

Patricio S. Letelier†

Departamento de Matemática Aplicada
Universidade Estadual de Campinas
13081-970, Campinas, S.P., Brazil

Abstract

Two families of models of rotating relativistic disks based on Taub-NUT and Kerr metrics are constructed using the well-known “displace, cut and reflect” method. We find that for disks built from a generic stationary axially symmetric metric the “sound velocity”, $(\text{pressure}/\text{density})^{1/2}$, is equal to the geometric mean of the prograde and retrograde geodesic circular velocities of test particles moving on the disk. We also found that for generic disks we can have zones with heat flow. For the two families of models studied the boundaries that separate the zones with and without heat flow are not stable against radial perturbations (ring formation).

PACS numbers: 04.20.Jb, 4.40.-b, 04.40.Dg, 04.20.-q

*e-mail: guillego@uis.edu.co

†e-mail: letelier@ime.unicamp.br

1 Introduction

Axially symmetric solutions of Einstein field equations corresponding to disk like configurations of matter are of great astrophysical interest and have been extensively studied. These solutions can be static or stationary and with or without radial pressure. Solutions for static disks without radial pressure were first studied by Bonnor and Sackfield [1], and Morgan and Morgan [2], and with radial pressure by Morgan and Morgan [3], and, in connection with gravitational collapse, by Chamorro, Gregory and Stewart [4]. Disks with radial tension has been recently considered in [5]. Also models of disks with, electric fields [6], magnetic fields [7], and both magnetic and electric fields have been introduced recently [8]. Using a solitonic technique Neugebauer and Meinel found solutions representing rigidly rotating disks of dust [9]. Several classes of exact solutions of the Einstein field equations that represent disks were obtained by different authors [10]-[18].

The stability of static models with no radial pressure can be explained by either assuming the existence of hoop stresses or that the particles on the disk plane move under the action of their own gravitational field in such a way that as many particles move clockwise as counterclockwise. This last interpretation is frequently made since it can be invoked to mimic true rotational effects. Even though, this interpretation can be seen as a device, there are observational evidence of disks made of streams of rotating and counter-rotating matter [19].

For disks without tension, i.e., usual fluid disks, the rotation is a necessary ingredient to have stability. Despite its relevance the literature on exact relativistic disks solutions to the Einstein field equations is scarce, we only found a discussion of a rotating disk as a source of Kerr metric [20].

The aim of this work is to study models of rotating relativistic disks in some detail. The models are based in Taub-NUT and Kerr metrics, that are some of the simplest axially symmetric stationary solutions of the vacuum Einstein equations [21]. To construct the disk solutions we use the well-known “displace, cut and reflect” method.

We find that for disks built from a generic stationary axially symmetric metric the “sound velocity”, $(pressure/density)^{1/2}$, is equal to the geometric mean of the prograde and retrograde geodesic circular velocities of a test particle moving on the disk. We also found that the generic disk may have zones with heat flow. For the two families of models studied the boundaries that separates the zones with and without heat flow are not stable against

radial perturbations (ring formation).

In Sec. II we study the generation of a disk model using the “displace, cut and reflect” method from a vacuum solution of the Einstein field equations for a stationary axially symmetric metric, in particular, we study: the general form of the associated energy-momentum tensor, disk velocity, and angular momentum. In the next section, Sec. III, we discuss the relation between the geodesic circular velocities on the disk and the pressure and density. In Sec. IV a class of models of rotating disks based on the Taub-NUT metric is presented. In particular, we study the apparition of heat flow and stability against radial perturbations. In Sec. V, another class of models of rotating disks is presented, this time based in the Kerr metric. Also the stability against radial perturbation is considered. The material presented here is complementary to the work of reference [20]. In the last section, Sec VI , we summarize our main results and made some comments.

2 Rotating Relativistic Disks

In this section we present a summary of the main quantities associated to the disk, we follow closely our reference [5]. A sufficiently general metric for our purposes is Weyl-Lewis-Papapetrou line element,

$$ds^2 = - e^{2\Phi}(dt + \mathcal{A}d\varphi)^2 + e^{-2\Phi}[r^2d\varphi^2 + e^{2\Lambda}(dr^2 + dz^2)], \quad (1)$$

where Φ , Λ and \mathcal{A} are functions of r and z only. Assuming the existence of the second derivatives of the functions Φ , Λ and \mathcal{A} , the Einstein vacuum equations for this metric are equivalent to,

$$\Phi_{,rr} + \frac{\Phi_{,r}}{r} + \Phi_{,zz} + \frac{e^{4\Phi}}{2r^2}(\mathcal{A}_{,r}^2 + \mathcal{A}_{,z}^2) = 0, \quad (2a)$$

$$\mathcal{A}_{,rr} - \frac{\mathcal{A}_{,r}}{r} + \mathcal{A}_{,zz} + 4(\Phi_{,r}\mathcal{A}_{,r} + \Phi_{,z}\mathcal{A}_{,z}) = 0, \quad (2b)$$

$$\Lambda_{,r} = r(\Phi_{,r}^2 - \Phi_{,z}^2) - \frac{e^{4\Phi}}{4r}(\mathcal{A}_{,r}^2 - \mathcal{A}_{,z}^2), \quad (2c)$$

$$\Lambda_{,z} = 2r\Phi_{,r}\Phi_{,z} - \frac{e^{4\Phi}}{2r}\mathcal{A}_{,r}\mathcal{A}_{,z}. \quad (2d)$$

Now if the first derivatives of the metric tensor are not continuous on the plane $z = 0$ with discontinuity functions,

$$b_{ab} = g_{ab,z}|_{z=0^+} - g_{ab,z}|_{z=0^-},$$

the Einstein equations yield an energy-momentum tensor (EMT) $T_{ab} = Q_{ab} \delta(z)$, where $\delta(z)$ is the usual Dirac function with support on the disk and

$$Q_b^a = \frac{1}{2} \{ b^{az} \delta_b^z - b^{zz} \delta_b^a + g^{az} b_b^z - g^{zz} b_b^a + b_c^c (g^{zz} \delta_b^a - g^{az} \delta_b^z) \}.$$

is the distributional energy-momentum tensor. The “true” surface energy-momentum tensor of the disk can be written as $S_{ab} = e^{\Lambda-\Phi} Q_{ab}$.

For the metric (1) we obtain

$$S_{00} = 2e^{3\Phi-\Lambda} [2\Phi_{,z} - \Lambda_{,z}], \quad (3a)$$

$$S_{01} = e^{3\Phi-\Lambda} [4\mathcal{A}\Phi_{,z} - 2\mathcal{A}\Lambda_{,z} + \mathcal{A}_{,z}] \quad (3b)$$

$$S_{11} = 2e^{3\Phi-\Lambda} [(r^2 e^{-4\Phi} - \mathcal{A}^2)\Lambda_{,z} + 2\mathcal{A}^2\Phi_{,z} + \mathcal{A}\mathcal{A}_{,z}] \quad (3c)$$

where all the quantities are evaluated at $z = 0^+$.

The eigenvalue problem for the energy-momentum tensor (3a) - (3c),

$$S_b^a \xi^b = \lambda \xi^a, \quad (4)$$

has the solutions

$$\lambda_{\pm} = \frac{1}{2} \left(T \pm \sqrt{D} \right), \quad (5)$$

and $\lambda_r = \lambda_z = 0$, where

$$T = S_0^0 + S_1^1, \quad D = (S_1^1 - S_0^0)^2 + 4 S_1^0 S_0^1. \quad (6)$$

We can write

$$g_{ab} = -V_a V_b + W_a W_b + X_a X_b + Y_a Y_b, \quad (7)$$

and the canonical form of the EMT,

$$S_{ab} = \sigma V_a V_b + P W_a W_b + K (V_a W_b + W_a V_b), \quad (8)$$

with a orthonormal basis

$$V^a = N_0(1, \Omega, 0, 0), \quad (9a)$$

$$W^a = N_1(\Delta, 1, 0, 0), \quad (9b)$$

$$X^a = e^{\Phi-\Lambda}(0, 0, 1, 0), \quad (9c)$$

$$Y^a = e^{\Phi-\Lambda}(0, 0, 0, 1), \quad (9d)$$

where N_0 and N_1 are normalization factors, and

$$\Omega = \begin{cases} (\lambda_- - S_0^0)/S_1^0 & , D \geq 0 , \\ (S_1^1 - S_0^0)/2S_1^0 & , D \leq 0 , \end{cases} \quad (10)$$

$$\Delta = \begin{cases} (\lambda_+ - S_1^1)/S_0^1 & , D \geq 0 , \\ 0 & , D \leq 0 , \end{cases} \quad (11)$$

The energy density, the azimuthal pressure, and the heat flow function are, respectively,

$$\sigma = \begin{cases} -\lambda_- & , D \geq 0 , \\ -T/2 & , D \leq 0 , \end{cases} \quad (12)$$

$$P = \begin{cases} \lambda_+ & , D \geq 0 , \\ T/2 & , D \leq 0 , \end{cases} \quad (13)$$

$$K = \begin{cases} 0 & , D \geq 0 , \\ \sqrt{-D}/2 & , D \leq 0 . \end{cases} \quad (14)$$

The orthonormal basis $\{V^a, W^a, X^a, Y^a\}$ is comoving with the disk. Thus the time-like vector V^a will define the velocity vector of the disk:

$$V^a = (V^0, V^1, 0, 0) = V^0(1, \Omega, 0, 0), \quad (15)$$

where

$$V^0 = \frac{e^{-\Phi}}{\sqrt{1 - V^2}}, \quad (16)$$

and

$$V = \sqrt{\frac{g_{11}\Omega^2 + 2g_{01}\Omega}{-g_{00}}} \quad (17)$$

is the tangential velocity of the disk.

The specific angular momentum of a particle of the disk, with mass μ , is given by

$$h = \frac{p_\varphi}{\mu} = g_{\varphi a} V^a. \quad (18)$$

Thus,

$$h = \frac{g_{11}\Omega + g_{01}}{\sqrt{-g_{00} - 2g_{01}\Omega - g_{11}\Omega^2}}. \quad (19)$$

A condition of stability under radial perturbations is

$$\frac{d(h^2)}{dr} = 2h \frac{dh}{dr} > 0, \quad (20)$$

For $h > 0$, we have stability when the specific angular momentum is an increasing function of r . This criteria is an extension of Rayleigh criteria of stability of a fluid at rest in a gravitational field, see for instance [22].

3 The counter-rotating Model

In this section we analyze the model of disks made of particles moving in opposite directions. When the discriminant D is positive there is not heat flow. Furthermore, when $P > 0$ an observer comoving with the disks can consider the energy-momentum tensor as representing two streams of collisionless particles that circulate in opposite directions.

Let be $u^a = (u^0, u^1, 0, 0) = u^0(1, \omega, 0, 0)$ the velocity vector of the stream. The angular velocity ω can be obtained from the geodesic equation for a test particle, we get

$$g_{11,r}\omega^2 + 2g_{01,r}\omega + g_{00,r} = 0, \quad (21)$$

with solutions,

$$\omega_{\pm} = \frac{-g_{01,r} \pm \sqrt{g_{01,r}^2 - g_{00,r}g_{11,r}}}{g_{11,r}}. \quad (22)$$

Therefore, in general, the two streams circulate with different velocities.

We can compute the tangential velocity of the streams by projecting the velocity vector u^a onto the comoving tetrad, $e_{\hat{a}}{}^b = \{V^b, W^b, X^b, Y^b\}$,

$$u^{\hat{a}} = e_{\hat{a}}{}^b u^b = \eta^{\hat{a}\hat{c}} e_{\hat{c}b} u^b. \quad (23)$$

We get,

$$U_{\pm} = \left| \frac{u^{\hat{1}}}{u^{\hat{0}}} \right| = \left| \frac{W_0 + W_1 \omega_{\pm}}{V_0 + V_1 \omega_{\pm}} \right|. \quad (24)$$

By performing the product of U_+ and U_- we obtain

$$U_+ U_- = \left| \frac{W_0^2 + W_0 W_1 (\omega_+ + \omega_-) + W_1^2 \omega_+ \omega_-}{V_0^2 + V_0 V_1 (\omega_+ + \omega_-) + V_1^2 \omega_+ \omega_-} \right|. \quad (25)$$

From (21) we have the relations,

$$\omega_+ + \omega_- = -\frac{2g_{01,r}}{g_{11,r}}, \quad \omega_+ \omega_- = \frac{g_{00,r}}{g_{11,r}}. \quad (26)$$

Thus,

$$U_+ U_- = \left| \frac{g_{11,r} W_0^2 - 2g_{01,r} W_0 W_1 + g_{00,r} W_1^2}{g_{11,r} V_0^2 - 2g_{01,r} V_0 V_1 + g_{00,r} V_1^2} \right|. \quad (27)$$

By using (7) and (8), we can write

$$U_+ U_- = \left| \frac{A + \sigma B}{A - PB} \right|, \quad (28)$$

where

$$A = g_{11,r} S_{00} - 2g_{01,r} S_{01} + g_{00,r} S_{11}, \quad (29a)$$

$$B = g_{00} g_{11,r} - 2g_{01} g_{01,r} + g_{00,r} g_{11}. \quad (29b)$$

Using the Einstein equations (2a) - (2d) and the expressions (3a) - (3c) for the energy-momentum tensor (with $K = 0$) we can show that

$$A = -2r(S_0^0 + S_1^1). \quad (30)$$

Also, using the metric (1) we get,

$$B = -2r. \quad (31)$$

Hence, assuming that $P > 0$ and $\sigma > 0$, we obtain

$$U_+U_- = \left| \frac{S_0^0 + S_1^1 + \sigma}{S_0^0 + S_1^1 - P} \right| \quad (32)$$

$$= \frac{P}{\sigma}. \quad (33)$$

In other words, for disks built from a generic stationary axially symmetric metrics the “sound velocity” $(P/\sigma)^{1/2}$ is equal to the geometric mean of the prograde and retrograde geodesic circular velocities of a test particle moving on the disk.

4 Taub-NUT Disks

The simplest stationary axially symmetric solution of the Einstein equations is the Taub-NUT solution that can be written as (1) with

$$\Phi = \frac{1}{2} \ln \left[\frac{x^2 - 1}{x^2 + 2px + 1} \right], \quad (34a)$$

$$\Lambda = \frac{1}{2} \ln \left[\frac{x^2 - 1}{x^2 - y^2} \right], \quad (34b)$$

$$\mathcal{A} = 2\alpha qy, \quad (34c)$$

where $p = m/\alpha$, $q = l/\alpha$, with $\alpha^2 = m^2 + l^2$, so that $p^2 + q^2 = 1$. m and l are the mass and the NUT parameter, respectively. x and y are the prolate spheroidal coordinates, given by

$$2\alpha x = \sqrt{r^2 + (z + b + \alpha)^2} + \sqrt{r^2 + (z + b - \alpha)^2}, \quad (35a)$$

$$2\alpha y = \sqrt{r^2 + (z + b + \alpha)^2} - \sqrt{r^2 + (z + b - \alpha)^2}, \quad (35b)$$

with $b > \alpha > 0$. Note that we have displaced the origin of the z -axis in b . From the above expressions we can compute the trace (T) and discriminant (D) of the energy-momentum tensor. We found $\tilde{T} = \alpha T$ and $\tilde{D} = \alpha^2 D$, with

$$\tilde{T} = -\frac{4\bar{y}[\bar{y}^2(2\bar{x}^3 + 3p\bar{x}^2 - p) + \bar{x}(p\bar{x}^3 - 3p\bar{x} - 2)]}{[(\bar{x}^2 - \bar{y}^2)(\bar{x}^2 + 2p\bar{x} + 1)]^{3/2}} \quad (36a)$$

$$\tilde{D} = \frac{16[\bar{y}^2(p\bar{x}^2 + 2\bar{x} + p)^2 - q^2\bar{x}^2(\bar{x}^2 - 1)(1 - \bar{y}^2)]}{(\bar{x}^2 - \bar{y}^2)(\bar{x}^2 + 2p\bar{x} + 1)^3}. \quad (36b)$$

\bar{x} and \bar{y} are given by

$$2\bar{x} = \sqrt{\tilde{r}^2 + (\kappa + 1)^2} + \sqrt{\tilde{r}^2 + (\kappa - 1)^2}, \quad (37a)$$

$$2\bar{y} = \sqrt{\tilde{r}^2 + (\kappa + 1)^2} - \sqrt{\tilde{r}^2 + (\kappa - 1)^2}, \quad (37b)$$

where $\tilde{r} = r/\alpha$ and $\kappa = b/\alpha$.

Even though we have an exact solution and all the relevant quantities of the disk can be explicitly computed the resulting expressions are cumbersome and not very illuminating, the adoption of the graphic method is more adequate in this case. The first quantity to be considered is the discriminant D that will give us the canonical form of the EMT.

In Fig. 1 we show \tilde{D} for Taub-NUT disks with different values of p and κ . First we plot \tilde{D} for disks with $\kappa = 1.7$ and $p = 0.9, 0.7, 0.5, 0.3,$ and 0.1 . Then we plot \tilde{D} for disks with $p = 0.8$ and $\kappa = 2, 2.6, 3.2, 3.8,$ and 4.4 . We also computed \tilde{D} for many other values of p and κ . We found that in all the cases when $p \neq 1$, D is not positive definite and it has only one root $\tilde{r}_0 > 0$. Therefore the Taub-NUT disks always have heat flow beginning at $\tilde{r} = \tilde{r}_0$.

In Fig 2 we depict the density $\tilde{\sigma} = \alpha\sigma$ and the pressure $\tilde{P} = \alpha P$ for Taub-NUT disks with different values of p and κ . First we plot $\tilde{\sigma}$ and \tilde{P} (scaled by a factor 10) for Taub-NUT disks with $\kappa = 1.4$ and $p = 1, 0.8,$ and 0.6 as functions of $\tilde{r} = r/m$. Then we plot $\tilde{\sigma}$ and \tilde{P} (scaled by a factor 10) for Taub-NUT disks with $\kappa = 1.7$ and $p = 1, 0.8,$ and 0.6 as functions of $\tilde{r} = r/m$. We also computed $\tilde{\sigma}$ and \tilde{P} for many other values of p and κ , in all the cases, we obtain a similar behaviour. The density $\tilde{\sigma}$ is always positive, $\tilde{\sigma} > 0$; whereas the pressure becomes negative (tension) for a value of $\tilde{r} < \tilde{r}_0$. We can also see that $\tilde{\sigma}$ and \tilde{P} presents a non smooth behaviour at $\tilde{r} = \tilde{r}_0$. For $\tilde{r} > \tilde{r}_0$ we have heat flow.

The heat flow function $\tilde{K} = \alpha K$ is represented in Fig. 3. We plot \tilde{K} for $\kappa = 1.4$ (upper two curves) and $\kappa = 1.7$ (lower two curves), with $p = 0.8$ and 0.6 as functions of \tilde{r} . Also in Fig. 3, in order to see the change of behaviour of $\tilde{\sigma}$ and \tilde{P} at $\tilde{r} = \tilde{r}_0$ and the relation between $\tilde{\sigma}$ and \tilde{K} , we plot $\tilde{\sigma}$, \tilde{P} and \tilde{K} for $\kappa = 1.1$ and $p = 0.8$ in the interval $2.5 \leq \tilde{r} \leq 3$. We can see that $\tilde{K} > \tilde{\sigma}$ for $\tilde{r} \geq \tilde{r}_1 > \tilde{r}_0$. Thus, there is not causal propagation of heat for $\tilde{r} > \tilde{r}_1$.

In Fig. 4 we show the tangential disk velocity V and the disk angular momentum h for Taub-NUT disks with $p = 0.8$ and $\kappa = 1.1, 1.4, 1.7$ and 2 , as functions of \tilde{r} . We see that there is a strong change in the slope of V and h at $\tilde{r} = \tilde{r}_0$. That means that there is a strong instability at this value of \tilde{r} . We also show the stream angular momenta h_+ and h_- in order to compare with the counter-rotating model. We also found instability, but in a different place. We computed also V and h for a wide range of the parameters p and κ , we found always the same behaviour.

In order to compare the counter-rotating model of the disk with the true disk rotation, we plot in Fig. 5 the tangential velocities of the counter-rotating streams, U_+ (top) and U_- , and the product U_+U_- (bottom full line) and the P/σ (full dots) for $\kappa = 1.1$ and $p = 0.8$, as functions of \tilde{r} . We can see the exact matching of the two curves, U_+U_- and P/σ , in perfect agreement with (33). Also in Fig. 5, in order to show the behavior of the counter-rotating model for the different disks models, we plot the P/σ relation for $\kappa = 1.4$ (upper curves) and $\kappa = 1.7$ (lower curves), with $p = 1, 0.8$, and 0.6 as functions of \tilde{r} .

5 Kerr Disks

In this section we use the “displace, cut, and reflect” method to built disk solutions using the Kerr solution, that can be written as (1) with

$$\Phi = \frac{1}{2} \ln \left[\frac{p^2 x^2 + q^2 y^2 - 1}{(px + 1)^2 + q^2 y^2} \right], \quad (38a)$$

$$\Lambda = \frac{1}{2} \ln \left[\frac{p^2 x^2 + q^2 y^2 - 1}{p^2(x^2 - y^2)} \right], \quad (38b)$$

$$\mathcal{A} = \frac{2\alpha q}{p} \left[\frac{(1 - y^2)(px + 1)}{p^2 x^2 + q^2 y^2 - 1} \right], \quad (38c)$$

where $p = \alpha/m$, $q = a/m$, with $\alpha^2 = m^2 - a^2$, so that $p^2 + q^2 = 1$. m and a are the mass and the Kerr parameter, respectively. x e y are, again, the prolate spheroidal coordinates, given by (35a) and (35b).

With the above expressions we can compute the trace and the discriminant of the energy-momentum tensor, that now can be written as $\tilde{T} = mT$ and $\tilde{D} = m^2D$, with

$$\begin{aligned} \tilde{T} &= \frac{4\bar{x}\bar{y}(\bar{x}^2 - 1)(1 - \bar{y}^2)}{p(\bar{x}^2 - \bar{y}^2)^2(p^2\bar{x}^2 + q^2\bar{y}^2 - 1)} \\ &- 2\bar{y} \left\{ \frac{2q^2\bar{x}(p\bar{x} + 1)(1 - \bar{y}^2) + p(\bar{x}^2 - 1)[(p\bar{x} + 1)^2 - q^2\bar{y}^2]}{p(\bar{x}^2 - \bar{y}^2)(p^2\bar{x}^2 + q^2\bar{y}^2 - 1)[(p\bar{x} + 1)^2 + q^2\bar{y}^2]} \right\} \end{aligned} \quad (39a)$$

$$\begin{aligned} \tilde{D} &= 4\bar{y}^2 \left\{ \frac{2q^2\bar{x}(p\bar{x} + 1)(1 - \bar{y}^2) + p(\bar{x}^2 - 1)[(p\bar{x} + 1)^2 - q^2\bar{y}^2]}{p(\bar{x}^2 - \bar{y}^2)(p^2\bar{x}^2 + q^2\bar{y}^2 - 1)[(p\bar{x} + 1)^2 + q^2\bar{y}^2]} \right\}^2 \\ &- \frac{16q^2\bar{y}^2(\bar{x}^2 - 1)(1 - \bar{y}^2)[3p^2\bar{x}^2 + 4p\bar{x} - q^2\bar{y}^2 + 1]^2}{p^2(\bar{x}^2 - \bar{y}^2)^2(p^2\bar{x}^2 + q^2\bar{y}^2 - 1)^3[(p\bar{x} + 1)^2 + q^2\bar{y}^2]}, \end{aligned} \quad (39b)$$

where \bar{x} and \bar{y} are given by

$$2p\bar{x} = \sqrt{\tilde{r}^2 + (\kappa + p)^2} + \sqrt{\tilde{r}^2 + (\kappa - p)^2}, \quad (40a)$$

$$2p\bar{y} = \sqrt{\tilde{r}^2 + (\kappa + p)^2} - \sqrt{\tilde{r}^2 + (\kappa - p)^2}, \quad (40b)$$

where $\tilde{r} = r/m$ and $\kappa = b/m$.

In Fig. 6 we show \tilde{D} for Kerr disks with different values of p and κ . We first plot \tilde{D} for disks with $\kappa = 1.5$ and $p = 1, 0.9, 0.8, 0.6$, and 0.3 . Then we show \tilde{D} for disks with $p = 0.8$ and $\kappa = 1.7, 2, 2.3, 2.9$, and 3.8 . We also computed \tilde{D} for different values of p and κ , we find that for some values of p and κ , $\tilde{D} > 0$ everywhere on the disk, whereas for the complementary case \tilde{D} have two roots, $0 < \tilde{r}_1 < \tilde{r}_2$, so that $\tilde{D} < 0$ when $0 < \tilde{r}_1 < \tilde{r}_2$. Accordingly we have two kinds of Kerr disks, ones with heat flow in an annular region ($0 < \tilde{r}_1 < \tilde{r}_2$) and others without heat flow.

We first analyze some cases when there is no heat flow. In Fig. 7 we show the density $\tilde{\sigma} = m\sigma$ and the pressure $\tilde{P} = mP$ for these Kerr disks. First we plot $\tilde{\sigma}$ and \tilde{P} (scaled by a factor 100) for a disk with $p = 0.9$ and $\kappa = 2.4, 2.5$, and 3 as functions of $\tilde{r} = r/m$. Then we plot $\tilde{\sigma}$ and \tilde{P} (scaled by a factor

10) for disks with $\kappa = 2.5$ and $p = 1, 0.9$, and 0.8 . We also computed $\tilde{\sigma}$ and \tilde{P} for a variety of p and κ , we found a similar behaviour. The density $\tilde{\sigma}$ is positive definite everywhere on the disk, falling to zero at infinity. There are values of p and κ such that the pressure \tilde{P} is positive definite, also falling to zero at infinity, whereas in other cases the pressure \tilde{P} is negative (tension) at the central region of the disks becoming positive for a value $\tilde{r}_0 > 0$; then falling to zero at infinity.

The rotational motion of these disks models is shown in Fig. 8. We first plot V for $p = 0.9$ with $\kappa = 2.4, 2.5$, and 3 and for $p = 0.8$ with $\kappa = 2.5$ (top curve) and then we plot the disk angular momentum h for the same values of p and κ . We can see that the disk velocity increases initially and then falls to zero at infinity and always is less than the light velocity. Also we see that the disk angular momentum is an increasing monotonic function of \tilde{r} . Thus these disks models are stable.

Finally, we analyze a Kerr disk with heat flow, with $p = 0.9$ and $\kappa = 1.5$. In Fig. 9 we show $\tilde{\sigma}$, \tilde{P} and \tilde{K} for this values of p and κ . We see that the density $\tilde{\sigma}$ is positive definite everywhere on the disk, falling to zero at infinity and that presents a change of slope at the values of \tilde{r} when $\tilde{D} = 0$, \tilde{r}_1 and \tilde{r}_2 . The pressure \tilde{P} is negative at the central region of the disk, becoming positive for a value of $\tilde{r} > \tilde{r}_2$. Also, \tilde{P} presents a change of slope at \tilde{r}_1 and \tilde{r}_2 . The heat flow function \tilde{K} increases rapidly and becomes larger than $\tilde{\sigma}$ for a value of $\tilde{r} > \tilde{r}_1$, \tilde{K} falls to zero, becoming less than $\tilde{\sigma}$ for a value of $\tilde{r} < \tilde{r}_2$. So, there is not causal propagation of heat on this region of the disk.

We also plot in Fig. 9 the disk angular momentum, h . We see that the angular momentum presents two instabilities, at the values of \tilde{r} when $\tilde{D} = 0$, \tilde{r}_1 and \tilde{r}_2 , and so the region of the disk where there is heat flow is highly instable. In order to see that these instabilities are present also in the counter-rotating model, we plot also the stream angular momenta, h_+ and h_- (scaled by a factor 20). We analyzed several other cases of Kerr disks with heat flow, we found the same behaviour.

6 Discussion

We presented two families of rotating disks based on the Taub-NUT and Kerr solutions. For the first family we find that the presence of heat flow is a generic property of this models, also generic is the radial instability produced by this flow. For the second family we find two sub classes one with and the

other without heat flow. The heat flow is concentrated in an annular region that is highly instable.

The relation found between the geodesic circular velocities and the “speed of sound” found is a generalization for the stationary case of the corresponding relation found by Morgan and Morgan [3] that is the base of the counter-rotating model.

The inclusion of current in the rotating models to have a rotating “hot” disk as the ones studied in [7] is under consideration. The rotation add mass to the otherwise massless charges. These models are quite nontrivial. Also, the inclusion of radial pressure or tension is being considered.

Finally, we want to mention that all the computation of this work was performed using the algebraic programming system Reduce [23].

Acknowledgments

We want to thank CNPq and FAPESP for financial support. Also G.A.G is grateful for the warm hospitality of the DMA-IMECC-UNICAMP where the main part of this work was performed.

References

- [1] W. A. Bonnor and A. Sackfield, *Comm. Math. Phys.* 8, 338 (1968)
- [2] T. Morgan and L. Morgan, *Phys. Rev.* 183, 1097 (1969)
- [3] L. Morgan and T. Morgan, *Phys. Rev. D* 2, 2756 (1970)
- [4] A. Chamorro, R. Gregory and J. M. Stewart, *Proc. R. Soc. Lond. A* 413, 251 (1987)
- [5] G. González and P. S. Letelier *Class. Quantum Grav.* 16, 479 (1999)
- [6] T. Ledvinka, M. Zofka and J. Bičák in “Proc. 8th Marcel Grossman Meeting in General relativity”, T. Piran ed. (World Scientific, Singapore 1999) pp. 339-341
- [7] P. S. Letelier, *Phys. Rev. D* 60, 104042-1 (1999)
- [8] J. Katz, J. Bičák, and D. Lynden-Bell, *Class. Quantum Grav.* 16, 4023 (1999)

- [9] G. Neugebauer and R. Meinel, *Phys. Rev. Lett.* 75, 3046 (1995)
- [10] P.S. Letelier and S. R. Oliveira, *J. Math. Phys.* 28, 165 (1987)
- [11] D. Lynden-Bell and S. Pineault, *Mon. Not. R. Astron. Soc.* 185, 679 (1978)
- [12] J. P. S. Lemos, *Class. Quantum Grav.* 6, 1219 (1989)
- [13] J. P. S. Lemos and P. S. Letelier, *Class. Quantum Grav.* 10, L75 (1993)
- [14] J. P. S. Lemos and P. S. Letelier, *Phys. Rev D* 49, 5135 (1994)
- [15] J. P. S. Lemos and P. S. Letelier, *Int. J. Mod. Phys. D* 5, 53 (1996)
- [16] C. Klein, *Class. Quantum Grav.* 14, 2267 (1997)
- [17] J. Bičák, D. Lynden-Bell and J. Katz, *Phys. Rev. D* 47, 4334 (1993)
- [18] J. Bičák, D. Lynden-Bell and C. Pichon, *Mon. Not. R. Astron. Soc.* 265, 126 (1993)
- [19] F. Bertola *et al.* *Ap. J.* 458, L67 (1996).
- [20] J. Bičák and T. Ledvinka, *Phys. Rev. Lett*, 71, 1669 (1993)
- [21] D. Kramer, H. Stephani, M. McCallum and E. Herlt. *Exact Solutions of Einstein's Field Equations* (Cambridge University Press, Cambridge 1980)
- [22] L.D. Landau and E.M. Lifshitz, “ Fluid Mechanics” (Addison-Wesley, Reading 1989), Chapter 3.
- [23] A.D. Hearn and J.P. Fitch, *REDUCE User's Manual* (Konrad-Zuse-Zentrum, Berlin 1998)

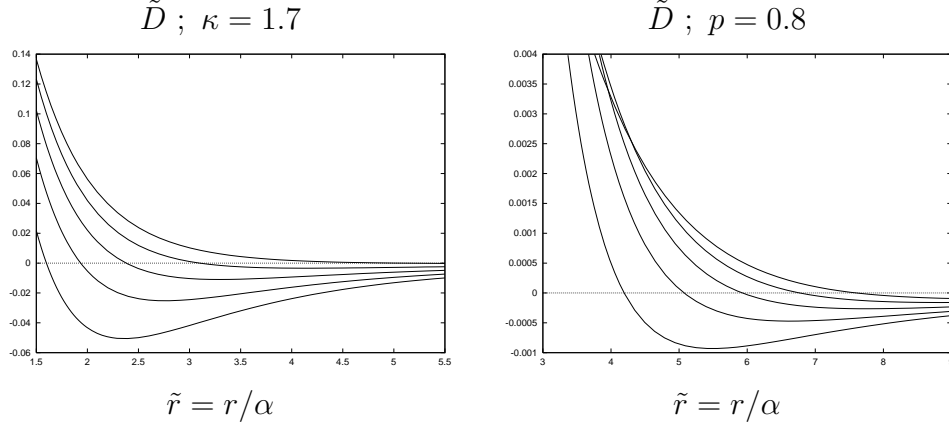


Figure 1: We plot \tilde{D} for Taub-NUT disks with $\kappa = 1.7$ and $p = 0.9, 0.7, 0.5, 0.3,$ and 0.1 as functions of $\tilde{r} = r/\alpha$. Next we plot \tilde{D} for Taub-NUT disks with $p = 0.8$ and $\kappa = 2, 2.6, 3.2, 3.8,$ and 4.4 as functions of $\tilde{r} = r/\alpha$. Note that D is not positive definite and has only one root $\tilde{r}_0 > 0$

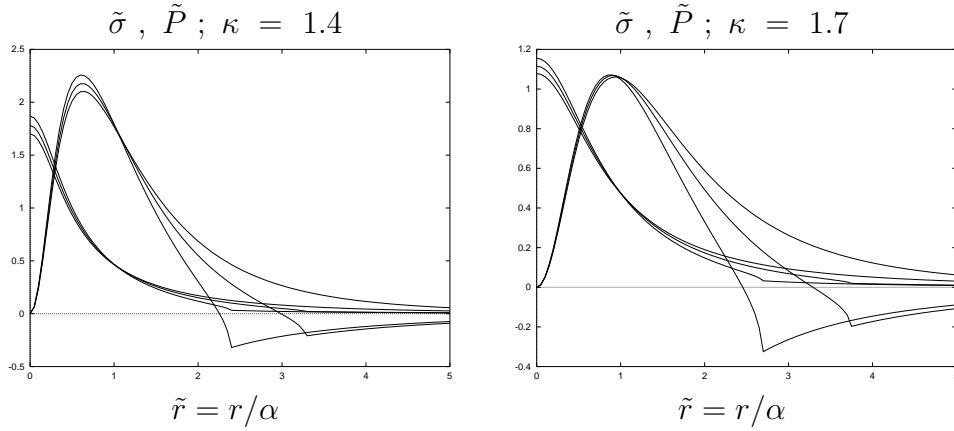


Figure 2: First we plot $\tilde{\sigma}$ and \tilde{P} (scaled by a factor 10) for Taub-NUT disks with $\kappa = 1.4$ and $p = 1, 0.8,$ and 0.6 as functions of $\tilde{r} = r/m$. Next we plot $\tilde{\sigma}$ and \tilde{P} (scaled by a factor 10) for a Taub-NUT disk with $\kappa = 1.7$ and $p = 1, 0.8,$ and 0.6 as functions of $\tilde{r} = r/m$. \tilde{P} presents a non smooth behaviour at $\tilde{r} = \tilde{r}_0$, wherein the heat flow begins.

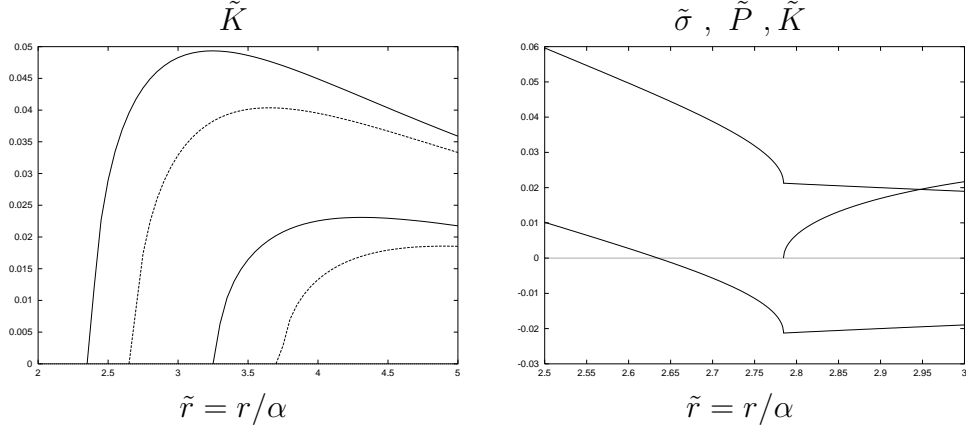


Figure 3: We show \tilde{K} for $\kappa = 1.4$ (upper curves) and $\kappa = 1.7$ (lower curves), with $p = 0.8$ and 0.6 as functions of \tilde{r} . Next we plot $\tilde{\sigma}$, \tilde{P} and \tilde{K} for $\kappa = 1.1$ and $p = 0.8$ in the interval $2.5 \leq \tilde{r} \leq 3$.

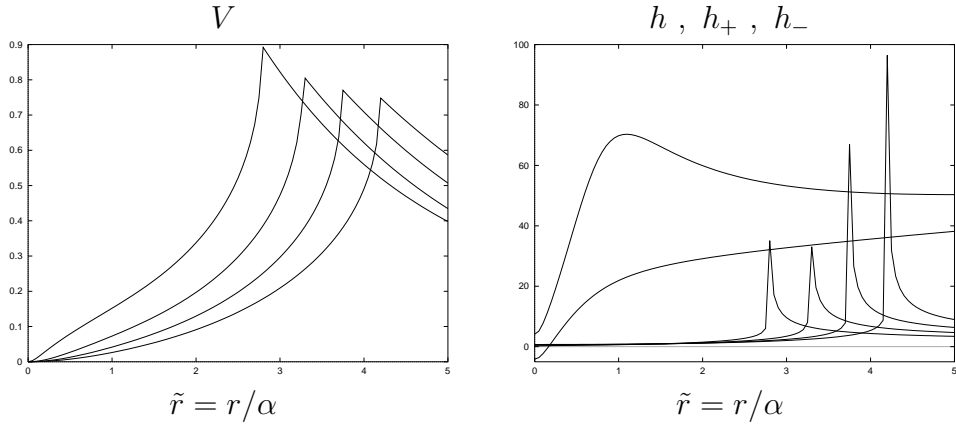


Figure 4: We plot the tangential disk velocity, V , with $p = 0.8$ and $\kappa = 1.1, 1.4, 1.7,$ and 2 as functions of \tilde{r} . Next we plot, for the same values of p and κ , the disk angular momentum, $-h$ (sharp curves), and the stream angular momenta, h_+ (top curve from the left) and $-h_-$ (scaled by a factor of 15), for $p = 0.8$ and $\kappa = 1.1$ as functions of \tilde{r} .

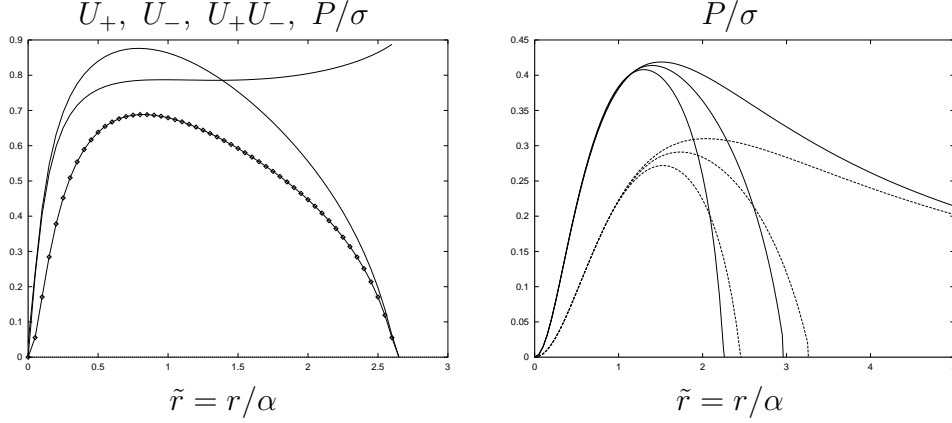


Figure 5: We show U_+ , U_- , U_+U_- and P/σ (full dots) for $\kappa = 1.1$ and $p = 0.8$ as functions of \tilde{r} . Next we plot the P/σ relation for $\kappa = 1.4$ (upper curves) and $\kappa = 1.7$ (lower curves), with $p = 1, 0.8$, and 0.6 as functions of \tilde{r} .

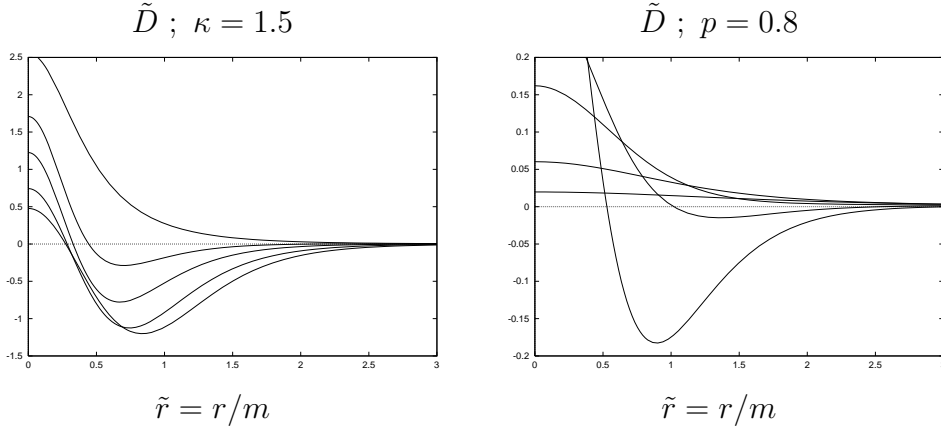


Figure 6: The discriminant \tilde{D} associated with the Kerr disks with $\kappa = 1.5$ is plotted for $p = 1, 0.9, 0.8, 0.6$, and 0.3 . Next we show \tilde{D} for disks with $p = 0.8$ and $\kappa = 1.7, 2, 2.3, 2.9$ and 3.8 . Note that \tilde{D} is not positive defined.

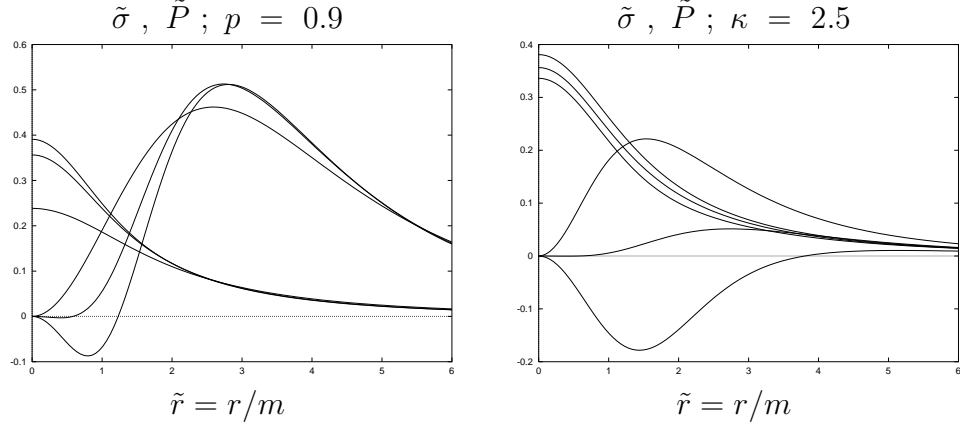


Figure 7: First we plot $\tilde{\sigma}$ and \tilde{P} (scaled by a factor of 100) for Kerr disks with $p = 0.9$ and $\kappa = 2.4, 2.5,$ and 3 as functions of $\tilde{r} = r/m$. Next we plot $\tilde{\sigma}$ and \tilde{P} (scaled by a factor of 10) for disks with $\kappa = 2.5$ and $p = 1, 0.9$ and 0.8 .

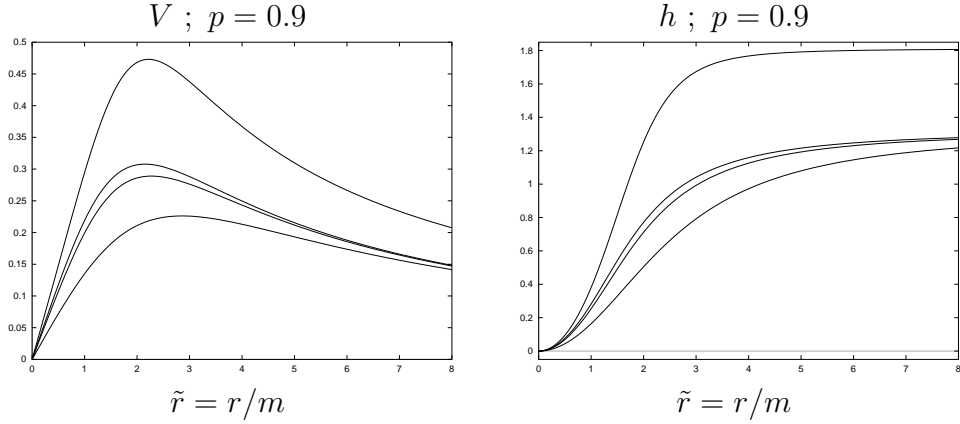


Figure 8: We plot V for $p = 0.8$ with $\kappa = 2.5$ (top curve) and $p = 0.9$ with $\kappa = 2.4, 2.5,$ and 3 (following three curves). Next we plot the disk angular momentum, h , for the same values of p and κ .

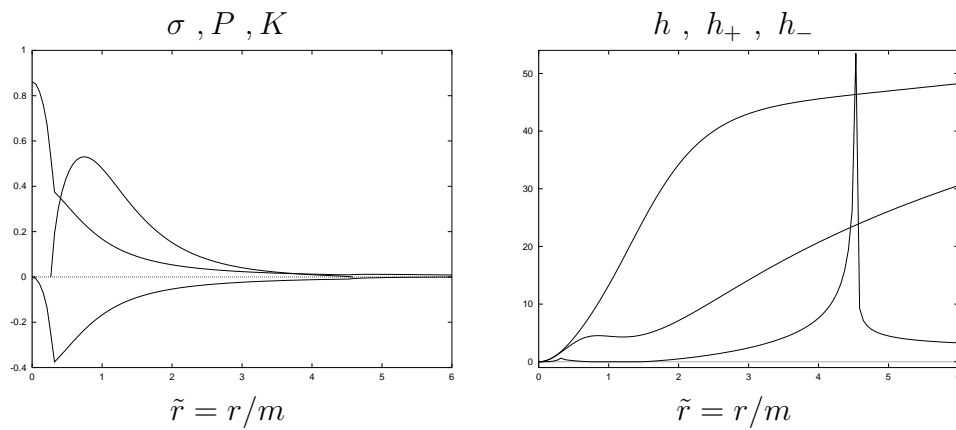


Figure 9: We plot the density, $\tilde{\sigma}$, the pressure, \tilde{P} , and the heat function, K , for a Kerr disk with $p = 0.9$ and $\kappa = 1.5$ as functions of $\tilde{r} = r/m$. Next, for the same values of p and κ , we plot the disk angular momentum, h , and the stream angular momenta, h_+ and h_- (scaled by a factor 20).